Journal of Applied Polymer Science

A Highly Efficient β-Nucleating Agent for Impact-Resistant Polypropylene Copolymer

Yi-Min Liu, Zai-Zai Tong, Jun-Ting Xu, Zhi-Sheng Fu, Zhi-Qiang Fan

MOE Key Laboratory of Macromolecular Synthesis and Functionalization, Department of Polymer Science & Engineering, Zhejiang University, Hangzhou 310027, China

Correspondence to: J.-T. Xu (E-mail: xujt@zju.edu.cn)

ABSTRACT: In this work, we reported calcium tetrahydrophthalate as a high efficient β-nucleating agent (β-NA) for impact-resistant polypropylene copolymer (IPC). The relative fraction of the β-crystal can reach as high as 93.5% when only 0.03% β-NA is added. The non-isothermal and isothermal crystallization behaviors, morphology, lamellar structure and mechanical properties of IPCs with various β-NA contents were studied. During non-isothermal crystallization, the cooling rate has an important influence on the relative fraction of the β-crystal, which decreases remarkably as the cooling rate increases. The β-NA also greatly accelerates crystallization rate of IPC, resulting from both more crystal nuclei and larger Avrami exponent. The small angle X-ray scattering characterization shows that more amorphous components are included into the inter-lamellae after addition of β-NA. Dynamical mechanical analysis (DMA) reveals that the storage modulus at low temperature and the loss factor above 0 °C from the PP component can be enhanced upon addition of β-NA and reach a maximum at the β-NA content of 0.05 wt %. Impact test shows that the impact strength of the IPC at 0°C can be improved as much as 40% when the content of calcium tetrahydrophthalate is 0.10 wt %. © 2014 Wiley Periodicals, Inc. J. Appl. Polym. Sci. **2014**, *131*, 40753.

KEYWORDS: crystallization; mechanical properties; morphology; polyolefins

Received 20 January 2014; accepted 21 March 2014

DOI: 10.1002/app.40753

INTRODUCTION

Impact-resistant polypropylene copolymer (IPC) is a type of isotactic polypropylene (iPP)-based in-reactor alloy with excellent balance in tensile and impact strengths. IPCs are widely used in many fields. Usually, IPCs are prepared by a two-stage or multi-stage polymerization process.[1,2] As a result, there exist various components in IPCs, including propylene homopolymer, ethylene-propylene random copolymer, ethylene-propylene multi-blocky copolymer, and minor polyethylene.[3–8] The complicated chain structure and multi-components in IPCs usually lead to a heterophasic structure, which is believed to be the origin of the better mechanical properties of IPCs. Many researches have been conducted to understand the structure-property of IPCs in the past two decades, including polymerization process,[9–13] structural analysis,[14–16] crystallization,[17,18] phase separation,[19–22] morphology,[23–28] and mechanical properties.[29–33]

For iPP homopolymer, nucleating agent (NA) is frequently added to improve the mechanical and optical properties. iPP may exhibit three different crystal modifications: α, β and γ. The β crystal is believed to have better impact property over the α crystal due to its unique crystal structure.[34,35] Therefore, to enhance the impact property of iPP, propylene copolymers, and iPP-containing blends, β nucleating agent (β-NA) is usually added.[36–38] As compared with the numerous literatures on β nucleation of iPP, there are few reports on β nucleation of IPCs.[39–42] Since IPCs are usually applied as impact-resistant materials, the impact property of IPCs is a key index for their application. Therefore, further improvement of the impact property of IPCs is necessary. Compared with modification in polymerization process, addition of β-NA is a more simple and efficient way. Recently, Fu and coworkers observed that the β-NA content significantly affected the impact strength of IPC at 0°C.[39] Wang and coworkers reported that the non-isothermal crystallization and multiple melting behaviors of IPC were affected by both cooling rate and β-NA content.[40] They also observed a synergistic effect between β-NA and processing melt temperature for the toughness of IPCs.[41] Feng and coworkers found that the brittle-ductile transition temperature of β-nucleated IPCs was lower than that of α-nucleated IPCs.[42] On the other hand, IPC is a multi-component system containing crystalline components. The crystallization kinetics and morphology of IPC depend on the relative rate of phase separation and crystallization,[19–22] which may be altered by addition of

Additional Supporting Information may be found in the online version of this article.

β-NA. From the viewpoint of interplay between crystallization and phase separation, it is also necessary to study the crystallization behavior of IPC in the presence of β-NA.

It has been reported that a lot of compounds, such as carboxylic acid/salt carboxylate,[43,44] polymers,[45,46] inorganic fillers,[47–50] aromatic amide,[51–55] rare earth compounds,[56,57] can act as β-NA of iPP. Nevertheless, many β-NAs are not highly efficient enough, because a large amount of β-NA is needed (> 1.0 wt %) or the content of the nucleated β-crystal is low (< 90%). In the present work, we reported a highly efficient β-NA, *i.e.* calcium tetrahydrophthalate,[58] for IPCs. The effects of this β-NA on crystallization, morphology and impact property of IPC were studied.

EXPERIMENTAL

Materials

Impact-resistant polypropylene copolymer (IPC) alloy (brand: J340) was provided by Yangzi Petrochemical Co., Ltd., Nanjing. The IPC sample was received in the form of powder without of any additive. The weight-average molecular mass (M_w) of IPC measured by GPC is 243 kg/mol and the molecular weight distribution (M_w/M_n) is 3.0. The weight percentage of the random copolymer (*n*-octane-soluble fraction at room temperature) is 16.2%. The antioxidant Irganox 1010 and β-NA (calcium tetraphthalate) were kindly donated by GCH Technology Co., Ltd., Guangzhou.

Preparation of the Samples

The powder of IPC was firstly mixed with prescribed amount of antioxidant and β-NA by hand at room temperature, then the mixture was fed into a Haake torque rheometer (Thermo Haake Rheomix, Thermo Haake Polylab System). The temperature inside the rheometer was 180°C, the rotating rate was 60 rpm and the mixing time is 8 min. After mixing, the blends were pelletized for next experiments. Five IPC samples with different β-NA contents (0.03, 0.05, 0.10, 0.20, and 0.30 wt %) were prepared. The content of antioxidant Irganox 1010 (0.5 wt %) was constant for each sample. IPC with 0.50 wt % antioxidant but no β-NA was used for control experiment.

Wide Angle X-ray Diffraction (WAXD)

Room temperature WAXD experiments were carried out on a Rigaku Dmax/2550PC X-ray diffractometer (Tokyo, Japan), operated at 40 kV and 40 mA. Ni-filtered CuKα radiation with a wavelength of 1.54 Å was used as the X-ray source. The range of diffraction angle for investigation was 2θ=5–35.0° and the scanning step is 0.0167°. The IPC samples were first held at 230°C for 5 min under thermal compression, then slowly cooled to room temperature in air. The obtained films of ~1 mm thickness were directly used for WAXD experiments without further treatment.

Differential Scanning Calorimetry (DSC)

DSC experiments were carried out on a TA Q200 calorimeter. About 3–5 mg of the samples was sealed with aluminum pans for each experiment. The samples were first heated to 230°C and held for 5 min to eliminate thermal history, then cooled to 30°C at pre-set cooling rate. For non-isothermal crystallization, different cooling rates, 2, 5, 10, and 20°C/min were applied. Subsequently the samples were again heated to 230°C at a rate of 10°C/min. The non-isothermal crystallization traces and the melting traces in the second run were recorded. For isothermal crystallization, the samples were cooled from 230°C to pre-set crystallization temperature (T_c=133°C) at a rate of 40°C/min, and held at T_c until crystallization was completed. The heat flow curves upon isothermal crystallization were recorded. After isothermal crystallization, the samples were directly heated from T_c=133°C to 200°C at a rate of 10°C/min to obtain the melting traces.

Small Angle X-ray Scattering (SAXS)

SAXS experiments were performed at BL16B1 beamline in Shanghai Synchrotron Radiation Facility (SSRF) in China. The wavelength was 1.24 Å and sample-to-detector distance was set as 2000 mm. Two-dimensional (2D) SAXS patterns were recorded at room temperature. The average exposure time was 300 s for each scan. Bull tendon was used as standard material for calibrating the scattering vector. The 2D SAXS patterns were converted into one-dimensional (1D) SAXS profiles using Fit2D software. Film samples for SAXS measurement were first isothermally crystallized at 133°C for 1 h.

Dynamic Mechanical Analysis (DMA)

Dynamic mechanical analysis measurements were performed on a DMA Q800 analyzer (TA instruments, USA) in the single cantilever mode. The rectangular shaped specimens with a size of 17.5 mm (length) × 12 mm (width) × 3 mm (thickness) were prepared by compression molding at 180°C followed by isothermal crystallization at 133°C for 1 h. The testing temperature ranged from −120°C to 100°C and the heating rate was 3°C/min. The oscillatory frequency was 1 Hz.

Impact Tests

The impact experiments were carried out according to CEAST (Ceast, Italy) at temperature of 0°C, with an impact speed of 3.46 m/s in a Charpy pendulum. Specimens with dimensions of 80 mm (length) × 10 mm (width) × 4 mm (thickness) for impact experiment were also prepared by thermal compression molding at 180°C followed by isothermal crystallization at 133°C for 1 h. The notches were prepared with a Ceast electrical notching apparatus at 20% of thickness and the angle of the "V" side groove was 45°. Impact properties were the average of at least 5 measurements.

RESULTS AND DISCUSSION

WAXD Result

The WAXD profiles of the IPCs with different β-NA contents are shown in Figure 1. One can see that the IPC containing no β-NA mainly exhibits the diffraction pattern of α-crystal with the peaks at 2θ=14.0°, 17.0°, 18.6°, and 21.9°, which correspond to the (110), (040), (130), and (131) + (041) reflections of α-crystal, respectively. Besides, the (300) reflection of β crystal is observed at 2θ=16.2° as well. As a result, α- and β-crystals co-exist in the neat IPC. However, we can see from the peak intensities that α-crystal is the majority and the β-crystal accounts for about 10% of the crystalline phase. It is well known that the β-crystal content in iPP is very low under common crystallization condition. The appearance of the β crystal

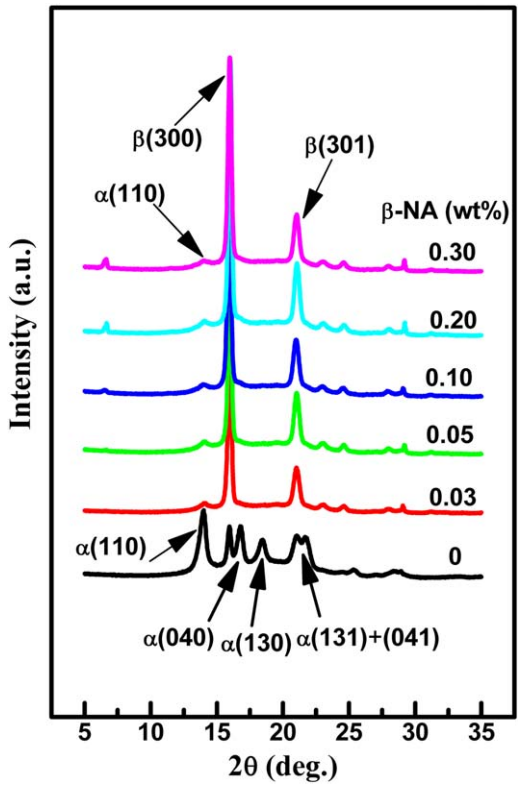

Figure 1. WAXD profiles of IPCs with various β-NA contents. [Color figure can be viewed in the online issue, which is available at wileyonlinelibrary.com.]

in the neat IPC is probably related to the compression moulding for preparation of the film samples. Shangguan et al. also observed the β-crystal in the compression-moulded iPP and they found that the β-crystal could be eliminated by re-heating and crystallization under quiescent condition.[59] After addition of only 0.03 wt % β-NA, the diffraction peaks of α-crystal become very weak and two peaks corresponding to (300) and (301) reflections of β-crystal are observed at $2\theta=16.2^\circ$ and 21.0°.

The crystallinity of IPCs can be calculated according to following equation:

$$X_c^{WAXD}=\frac{\sum A_c}{\sum A_c+\sum A_a}\times 100\% \quad (1)$$

where X_c^{WAXD} is the overall crystallinity calculated from WAXD pattern, A_c is the total area of crystalline peaks, and A_a is the total area of amorphous peaks.

The relative fractions of α- and β-crystals are calculated as following[60]:

$$K_\alpha^{WAXD}=\frac{\sum A_\alpha}{\sum A_\alpha+\sum A_\beta}\times 100\% \quad (2)$$

$$K_\beta^{WAXD}=\frac{\sum A_\beta}{\sum A_\alpha+\sum A_\beta}\times 100\% \quad (3)$$

where ΣA_α and ΣA_β are the total areas of crystalline peaks of α- and β-crystals, respectively.

The calculated relative fractions of α- and β-crystals (K_α^{WAXD} and K_β^{WAXD}) and the overall crystallinity (X_c^{WAXD}) are listed in Table I. The data in Table I show that, as the β-NA content increases, there is no evident change for the overall crystallinity. As compared with the IPC without β-NA, the overall crystallinity even becomes a little smaller at low level of β-NA content. After addition of very small amount of β-NA (0.03 wt %), there is a sharp change for both K_α^{WAXD} and K_β^{WAXD}. The value of K_β^{WAXD} increases from 10.9% for the neat IPC to 93.5% for the sample containing 0.03 wt % β-NA, whereas the value of K_α^{WAXD} decreases from 89.1% to 6.5% accordingly. This shows that the β-NA used in the present work is highly efficient to induce formation of β-crystal. With further increase of the β-NA content, K_α^{WAXD} decreases only slightly and K_β^{WAXD} increases a little.

Effect of Cooling Rate on Fraction of β-Crystal

It is reported that the cooling rate has a strong influence on the fraction of β-crystal in IPC.[40] In the present work, we also studied the effect of cooling rate on the fraction of β-crystal when IPCs are cooled from the melt. Four different cooling rates, 2, 5, 10, and 20°C/min, were applied to the samples. Figure 2 shows the DSC melting traces of different samples after cooling from 230°C at rates of 2 and 20°C/min, respectively. The corresponding DSC cooling curves are given in the supplementary material (Supporting Information Figure S1). After cooling from the melt at a rate of 2°C/min, double melting peaks are observed: one peak around 150°C and the other in range of 164–170°C [Figure 2(a)]. The melting peak at higher temperature can be assigned to α-crystal and the melting peak at lower temperature is attributed to β-crystal, since α-PP crystal usually has a higher melting temperature than β-PP crystal. For the IPC containing no β-NA, the melting peak at 164°C is dominant, whereas the melting peak of β-crystal is very weak and appears only as a shoulder. By contrast, after addition of β-NA, the melting peak of β-crystal becomes the major peak and the melting peak of α-crystal is the minority. This agrees well with the WAXD result that only a very small amount of β-NA can greatly promote formation of β-crystal. However, the melting DSC traces of IPCs cooled from the melt at a rate of 20°C/min show that the melting peak of α-crystal becomes obviously stronger [Figure 2(b)]. This indicates that the amount of β crystal becomes smaller at a faster cooling rate. It is reported that the crystallization rates of α- and β-crystals vary with crystallization temperature and β-crystal has a faster crystallization rate only in a suitable temperature window.[61] When the cooling rate is faster, the staying time for crystallization of β-crystal in this temperature window is shorter, thus fewer β-crystals are formed. The overall crystallinity (X_c^{DSC}) and the relative fraction of β-crystal (K_β^{DSC}) can also be calculated from the fusion enthalpy[62]:

$$X_c^{DSC}=\left[\frac{\Delta H_f(\alpha)}{209}+\frac{\Delta H_f(\beta)}{196}\right]\times 100\% \quad (4)$$

$$K_\beta^{DSC}=\frac{\Delta H_f(\beta)/196}{X_c^{\mathrm{DSC}}}\times 100\% \quad (5)$$

where $\Delta H_f(\alpha)$ and $\Delta H_f(\beta)$ are the fusion enthalpies of α- and β-crystals measured by DSC, respectively. The numbers of 209

Table I. The Data of Crystallinity for IPC Samples with Various β-NA Contents

Sample	β-NA content (wt %)	K_α^{WAXD} (%)	K_β^{WAXD} (%)	X_c^{WAXD} (%)
1	0	89.1	10.9	65.4
2	0.03	6.5	93.5	60.3
3	0.05	6.2	93.8	61.4
4	0.1	5.7	94.3	62.9
5	0.2	5.4	94.6	64.8
6	0.3	5.2	94.8	66.4

and 196 are the fusion enthalpies of α- and β-crystals of 100% crystallinity with a unit of J/g.

Figure 3 shows the variations of K_β^{DSC} with cooling rate for IPCs with different β-NA contents. It is observed that the relative fraction of β-crystal indeed decreases with increasing in cooling rate. This result is different from that reported by Wang and coworkers.[40] They observed that the relative fraction of β-crystal slightly increases with the cooling rate when the cooling rate is smaller than 20°C/min. We speculate that this difference originates from the different nucleation abilities of the β-NAs. Moreover, we also notice that the difference in K_β^{DSC} among IPCs with different β-NA contents also becomes larger at faster cooling rates. It is also observed that the melting temperature of the β-crystal increases slightly with the β-NA content (Figure 2). This shows that more β-NA can lead to formation of more perfect β-crystal with higher melting temperature during non-isothermal crystallization process.

Isothermal Crystallization Kinetics

The isothermal crystallization behavior of IPCs containing calcium tetrahydrophthalate as β-NA was also studied. Figure 4 shows the heat flow curves of IPCs with different β-NA contents isothermally crystallized at 133°C. It is observed that the heat flow of IPC with no β-NA reaches constant after 30 min. It should be noted that the α-crystal is dominant in this sample due to absence of β-NA. After addition of a small amount of β-NA (0.03 wt %), the heat flow becomes invariant after 15 min, indicating a much faster crystallization rate than that of IPC with no β-NA. The time corresponding to the maximum of heat flow exhibit a similar tendency. With further increase of the β-NA content, the peak of the heat flow shifts to shorter time, showing that the crystallization rate becomes faster.

The isothermal crystallization kinetics of semicrystalline polymers can be dealt with Avrami theory:

$$1-X(t)=\frac{\Delta H_{t=\infty}^c-\Delta H_t^c}{\Delta H_{t=\infty}^c-\Delta H_{t=0}^c}=\exp\left(-kt^n\right) \quad (6)$$

where $X(t)$ is the relative crystallinity at time t, and $\Delta H_{t=\infty}^c$, $\Delta H_{t=0}^c$, and ΔH_t^c are the crystallization enthalpies on complete crystallization ($t=\infty$), at $t=0$, and after time t, respectively. Therefore, we have:

$$\log\{-\ln[1-X(t)]\}=\log k+n\log t \quad (7)$$

The crystallization rate constant k and Avrami exponent n can be determined from the intercept and slope in the plot of log{-ln[1-$X(t)$]} versus log$t$, respectively. The crystallization half-time $t_{1/2}$ can be obtained from the following equation:

$$\log(t_{1/2})=[\log(\ln 2)-\log k]/n \quad (8)$$

Figure 5 shows the variation of $t_{1/2}$ with β-NA content at $T_c=133$°C. It can be seen from Figure 5 that the value of $t_{1/2}$ decreases with increasing in the β-NA content. Especially, there is a remarkable difference in $t_{1/2}$ between the neat IPC and β-nucleated IPCs. Crystallization half-time is an indication of overall crystallization rate. A smaller $t_{1/2}$ implies a faster overall crystallization rate. As a result, the data in Figure 5 shows that the β-nucleated IPCs crystallize much faster than the neat IPC and the overall crystallization rate of IPCs increases with the β-NA content. Because of this, pre-phase-separation in the melt

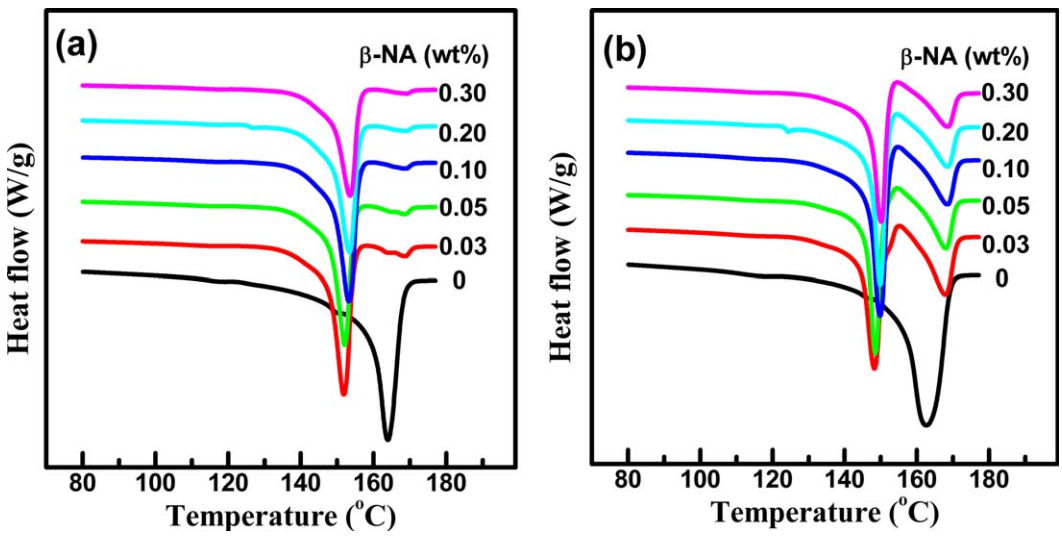

Figure 2. Melting DSC traces of IPCs with various β-NA contents after cooling from the melt at different cooling rates: 2°C /min (a) and 20°C /min (b). [Color figure can be viewed in the online issue, which is available at wileyonlinelibrary.com.]

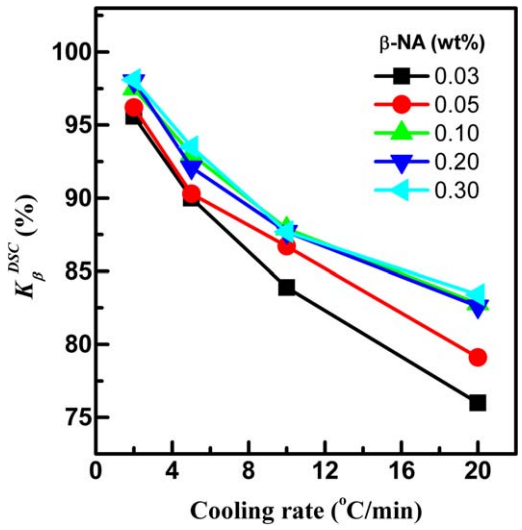

Figure 3. Plots of the relative fraction of β-crystal versus cooling rate during non-isothermal crystallization process of IPCs with various β-NA contents. [Color figure can be viewed in the online issue, which is available at wileyonlinelibrary.com.]

has no effect on the crystallization kinetics of IPC in the presence of β-NA, which is contrary to the result for the neat IPC.[19–22]

The Avrami plots for IPCs with various β-NA contents are shown in Figure 6. One can see that the slopes of the β-nucleated IPCs are evidently larger than that of the IPC without β-NA, which is verified by the obtained Avrami exponents. The IPC containing no β-NA has a relatively smaller Avrami exponent, which is also reported for other IPCs in our previous work.[21] The Avrami exponent is related to nucleation and crystal growth mechanisms. When the nucleation mechanism (heterogeneous nucleation) is the same, the larger Avrami exponent indicates a larger growth dimension of the formed crystal.

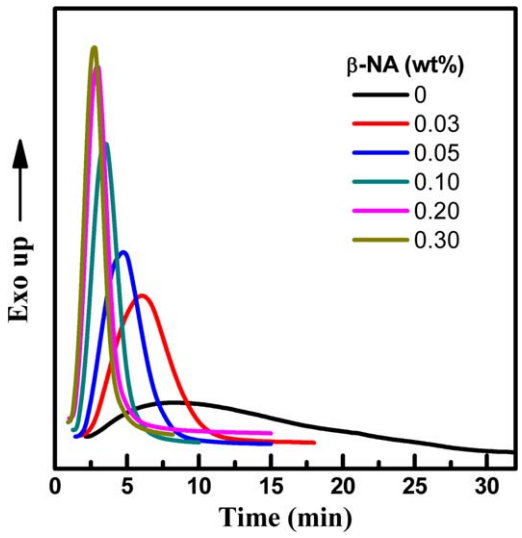

Figure 4. DSC heat flow curves for IPCs with different β-NA contents isothermally crystallized at 133°C. [Color figure can be viewed in the online issue, which is available at wileyonlinelibrary.com.]

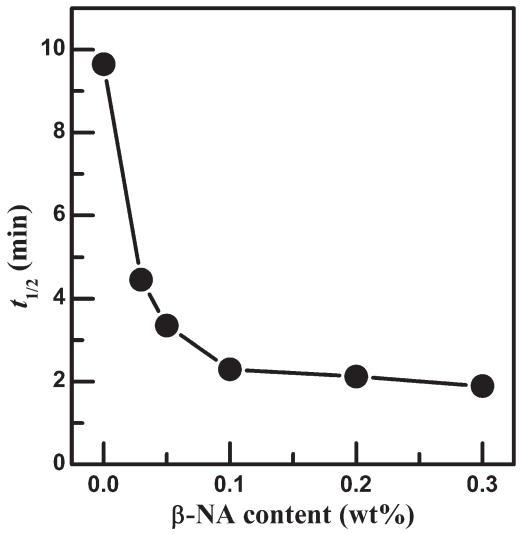

Figure 5. Variation of crystallization half-time at T_c=133°C with the β-NA content.

Therefore, the crystal growth dimension in the β-nucleated IPCs is larger than that in the neat IPC, which will be further confirmed by the macroscopic morphology in the next section. Moreover, as can be seen from eq. (8), a larger Avrami exponent (n) will lead to a smaller $t_{1/2}$, *i.e.*, faster crystallization rate. As a result, the larger growth dimension of the β-nucleated IPCs is one of the factors responsible for their faster crystallization rate.

Figure 7 shows the DSC melting traces after isothermal crystallization at T_c=133°C. It is found that the melting peak of all the IPCs nucleated by calcium tetrahydrophthalate is located at 154–155°C, corresponding to the melting temperature of β-crystal. By contrast, the IPC without β-NA exhibits a melting temperature of 169°C, which is the melting temperature of α-crystal. When the β-NA content is low, such as 0.03% and 0.05%, there exists a minor melting peak at higher temperature, indicating the presence of a very small amount of α-crystal.

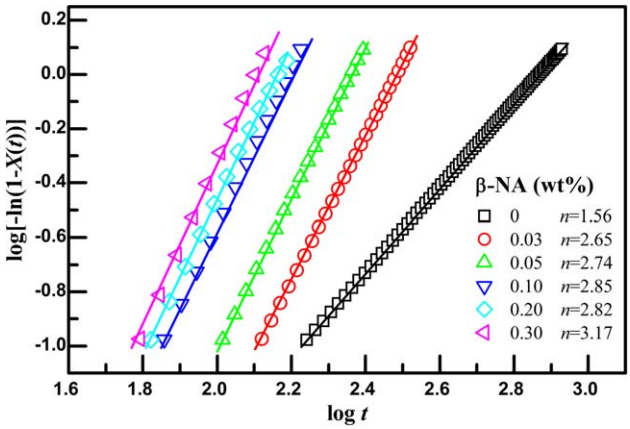

Figure 6. Avrami plots for IPCs with different β-NA contents at T_c=133°C. The Avrami exponents are indicated in the figure. [Color figure can be viewed in the online issue, which is available at wileyonlinelibrary.com.]

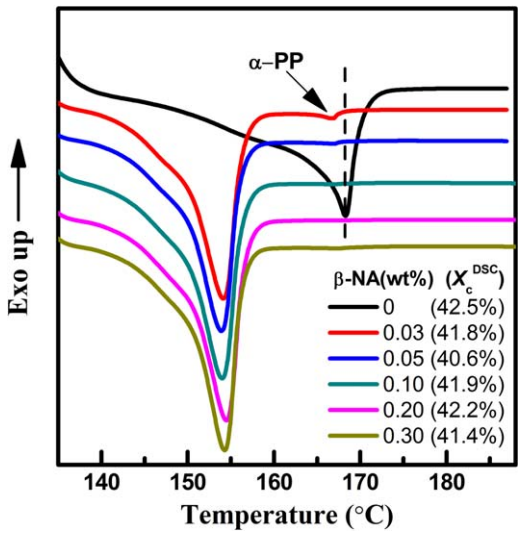

Figure 7. DSC heating curves of IPCs with various β-NA contents after isothermal crystallization at T_c=133 °C. The crystallinities calculated from the fusion enthalpy are also presented in the figure. [Color figure can be viewed in the online issue, which is available at wileyonlinelibrary.com.]

This shows that β-crystal is predominantly formed when IPCs isothermally crystallize at T_c=133°C in the presence of β-NA. The data of crystallinity after isothermal crystallization at T_c=133°C are calculated based on the fusion enthalpy and presented in Figure 7 as well. It is found that there is no evident difference in crystallinity among the β-IPCs. However, the calculated values of overall crystallinities (X_c^{DSC}) in Figure 7 are evidently smaller than those of X_c^{WAXD} measured by WAXD for compression-moulded samples in Table I. This difference originates from two aspects. Firstly, the crystallinity measured by density or WAXD is usually larger than that measure by DSC for the sample.[63–65] Secondly, parts of polymer chains of weaker crystallizability, such as the fraction with a multi-block structure, are difficult to crystallize at a high T_c.

Morphology

Since it is generally believed that NA can enhance the number of the crystal nuclei, the morphology of IPCs in the initial crystallization period is studied. Figure 8 shows the POM images of IPCs with various β-NA contents after isothermal crystallization at T_c=133°C for 2 min. Because of the short crystallization time, the size of crystallites is still quite small and the number of the crystallites can reflect that of the nuclei in the initial crystallization period. One can see from Figure 8 that there are few nuclei for the IPC without β-NA. After addition of β-NA, bundle-like crystal nuclei appear. The number of nuclei increases gradually as the β-NA content increases. This shows that, besides the larger Avrami exponent, the larger number of nuclei is also one of the major factors responsible for the faster crystallization of IPCs containing β-NA.

The morphology of IPCs after complete crystallization at T_c=133°C is also investigated, as shown in Figure 9. It is observed that small crystallites are formed when no β-NA is added. Such morphology agrees with its smaller Avrami exponent, which indicates a lower growth dimension of the crystals. This is possibly due to the effect of phase separation, which restricts the growth of PP crystals. When a very small amount of β-NA (0.03%) is added, some crystals of large size can be observed. Accordingly, the Avrami exponent becomes evidently larger. This implies that β-NA may weaken the confinement effect of phase separation.[21] Further work dealing the competition between NA and phase separation on crystallization of IPCs is still in progress. At low β-NA content, large and small crystals co-exist and non-uniform morphology is observed. At high β-NA content, uniform morphology is formed and the crystal size becomes a little smaller, but it is still larger than that in the IPCs without β-NA. The melting process of IPCs with various β-NA content was also monitored with POM after isothermal crystallization at T_c=133°C. The POM images upon heating were presented in the supplementary material (Supporting Information Figure S2). It is found that the crystals in the IPC with no β-NA start to disappear at very high temperature (164°C), whereas the crystals in the IPCs containing β-NA start to melt at a much lower temperature (153°C). Correspondingly, the end melting temperature of the β-crystal (165°C) is also lower than that of the α-crystal (175°C). This result is in accordance with the different melting temperatures of α- and β-crystals in Figure 7.

SAXS Result

The β-nucleated IPCs were characterized with SAXS. Figure 10(a) shows the Lorentz-corrected one-dimensional SAXS profiles of IPCs with different β-NA contents after isothermal crystallization at T_c=133°C. One can see that, as the content of β-NA increases, the scattering peak becomes weaker and slightly shifts to lower q. Since there is no big difference in crystallinity between the IPCs with and without β-NA, the lower scattering intensity of β-nucleated IPCs is probably due to the smaller density of β crystal than that of α crystal, leading to a smaller electron density difference between the crystalline and amorphous phases. The long period (L) can be calculated by $L=2\pi/q_{max}$, where q_{max} is scattering vector of the peak. The variation of the long period with β-NA contents is shown in Figure 10(b). We can see that the long period of the IPC with 0.03 wt % β-NA is much larger than that of the IPC containing no β-NA. This difference originates from the different crystal modifications in these two samples. With further increase in β-NA, the long period increases slightly. The long period is the sum of the thicknesses of the lamellar crystals and amorphous layer, if a two-phase model can be applied for the crystal structure of polymers. Because the β-crystals in different IPCs have similar melting temperatures (Figure 7), the lamellar crystal thicknesses are similar. As a result, we can conclude that more amorphous components are included into inter-lamellae of crystals. This is possibly because the crystallization rate is faster in the presence of β-NA and there is no enough time for the exclusion of the amorphous component outside the crystallites. Similar result was also reported by Feng and coworkers.[42] It should be noted that, the amorphous components in polymers of low crystallinity, such as IPCs, can be located both outside the macroscopic crystals and among the inter-lamellae.[64–66] SAXS can only measure the amount of the amorphous components included into the inter-lamellae, while the amorphous components outside

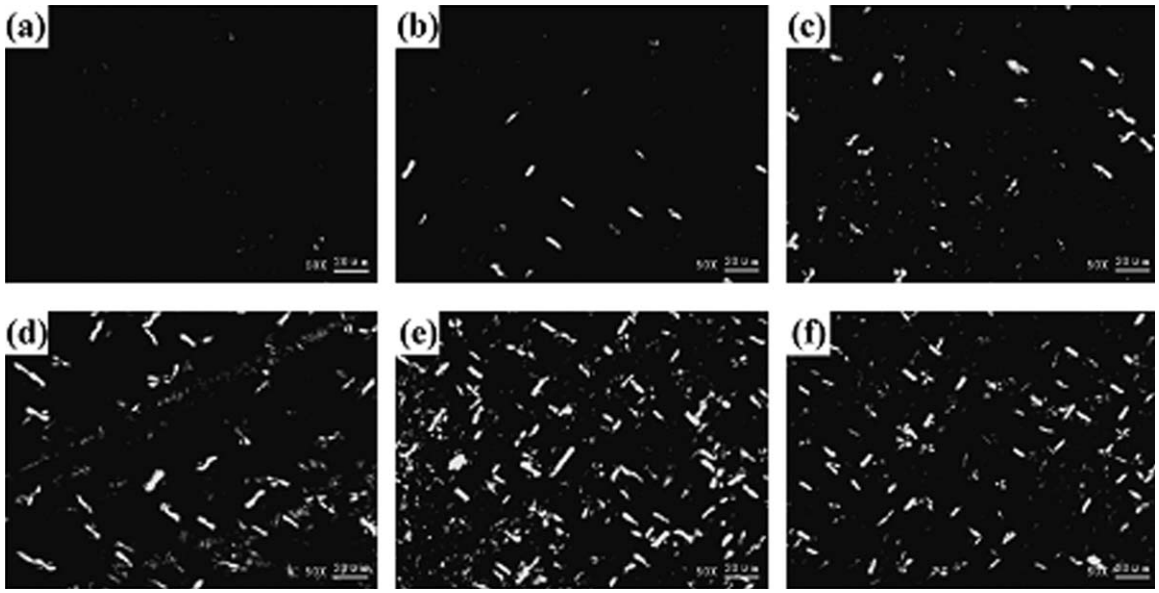

Figure 8. POM images of IPCs after isothermal crystallization at T_c=133°C for 2 min. The β-NA contents are 0 (a); 0.03 wt % (b); 0.05 wt % (c); 0.10 wt % (d); 0.20 wt % (e), and 0.30 wt % (f), respectively.

the macroscopic crystals cannot be probed by SAXS due to the large domain size. More inclusion of the amorphous components into the inter-lamellae means that the components outside the macroscopic crystals become fewer, since the overall crystallinity remains similar for different IPCs.

DMA Result

DMA testing was performed for IPCs with various β-NA contents in the temperature range of −120°C–100°C. The storage modulus (E') and loss factor (tanδ) of different samples are shown in Figure 11. It can be seen from Figure 11(a) that the IPCs with various β-NA contents have similar storage moduli at high temperature, but different storage moduli at low temperature. At low temperature, the storage modulus first increases with the β-NA content, and reaches a maximum at 0.05 wt % β-NA, then the storage modulus decreases with further increase of the β-NA content. The enhancement of storage modulus after addition of β-NA is out of our expectation, since the α-crystal possesses higher rigidity and strength than the β-crystal. This can be interpreted in terms of the SAXS result. As pointed out previously, the amorphous components can be located both outside the macroscopic crystals and among the inter-lamellae. The soft amorphous component outside the macroscopic crystals may greatly reduce the modulus upon deformation, while

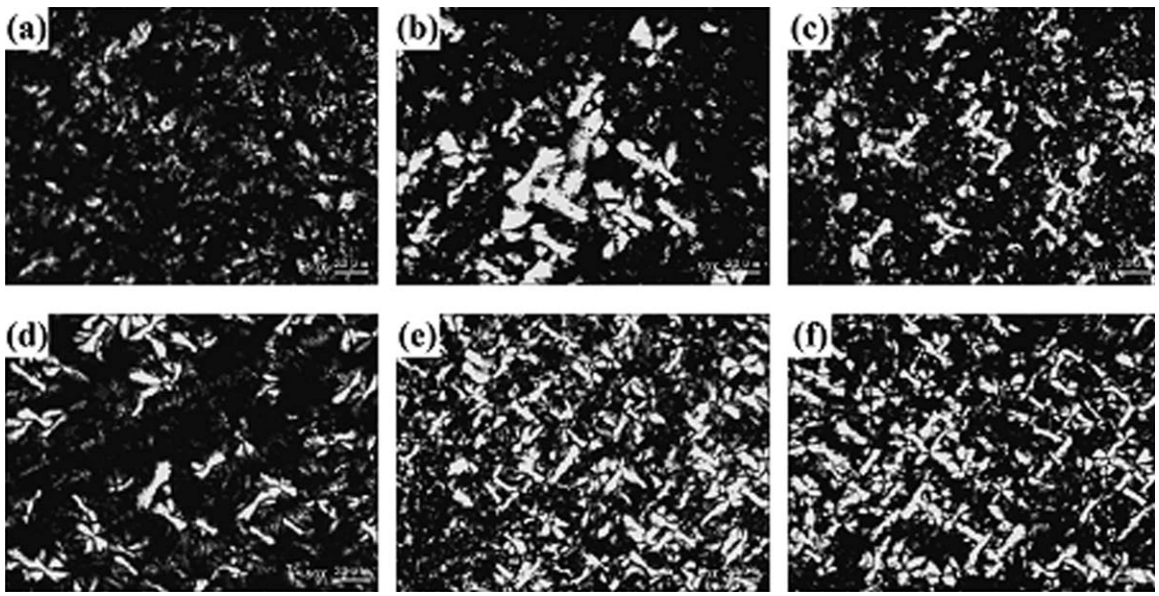

Figure 9. POM images of IPCs with various β-NA contents after complete crystallization at T_c=133°C. The β-NA contents are 0 (a); 0.03 wt % (b); 0.05 wt % (c); 0.10 wt % (d); 0.20 wt % (e), and 0.30 wt % (f), respectively.

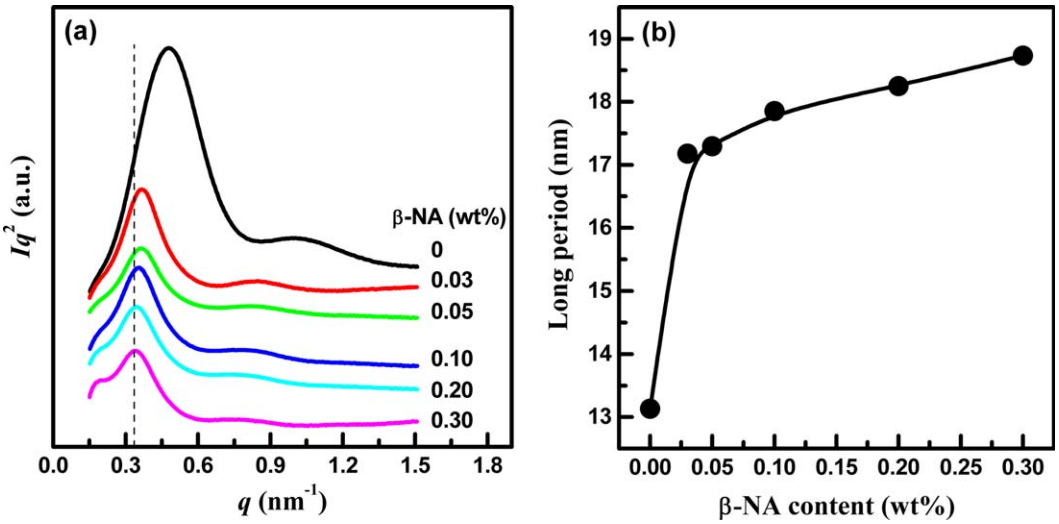

Figure 10. SAXS profiles and long periods for IPCs with various β-NA contents. [Color figure can be viewed in the online issue, which is available at wileyonlinelibrary.com.]

the amorphous components included into the inter-lamellae may contribute less to the modulus because they are surrounded by the hard crystalline lamellae. The SAXS result reveals that more amorphous components are included into the inter-lamellae after addition of β-NA, thus the storage modulus is increased.

As for the loss factor, two peaks are observed [Figure 11(b)] at $-30°C$ and $-22°C$, respectively. The low temperature peak is attributed to the glass transition of ethylene-propylene random copolymer (EPR) in IPCs. On the other hand, the high temperature peak corresponds to the glass transition of amorphous PP. As we know, IPC is usually produced by a two-stage polymerization process. In the first stage, propylene homopolymerization is performed and ethylene-propylene copolymerization is carried out in the second stage. As a result, IPC is a multi-component system, which contains PP homopolymer, EPR, ethylene-propylene multi-blocky copolymer and even a small amount of PE. It can be seen from Figure 11(b) that β-NA has little effect on the intensity of tanδ peak from EPR. This is quite normal, since EPR cannot crystallize. By contrast, the tanδ peak corresponding to PP changes greatly with the β-NA content. The intensity of the tanδ peak from PP first increases with the β-NA content, and the IPCs with 0.05 and 0.10 wt % of β-NA exhibit the strongest tanδ peak. With further increase of the β-NA content, the intensity of the tanδ peak from PP decreases gradually. This result is similar to that of the storage modulus of β-nucleated IPC at low temperature. Since the different IPCs have similar crystallinity, the change of the tanδ peak intensity from PP is attributed to the addition of β-NA, which alters the crystal structure and the amount of the amorphous components included into the inter-lamellae.

Impact Property

Figure 12 shows the Charpy impact strengths of IPCs with various β-NA contents after isothermal crystallization at T_c=133°C.

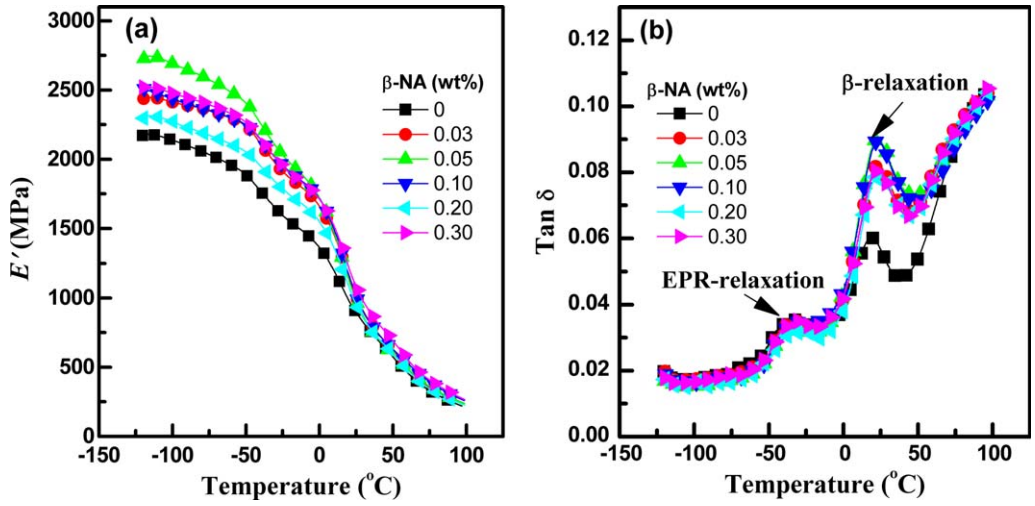

Figure 11. Storage moduli and loss factors (tanδ) of IPCs with various β-NA contents. [Color figure can be viewed in the online issue, which is available at wileyonlinelibrary.com.]

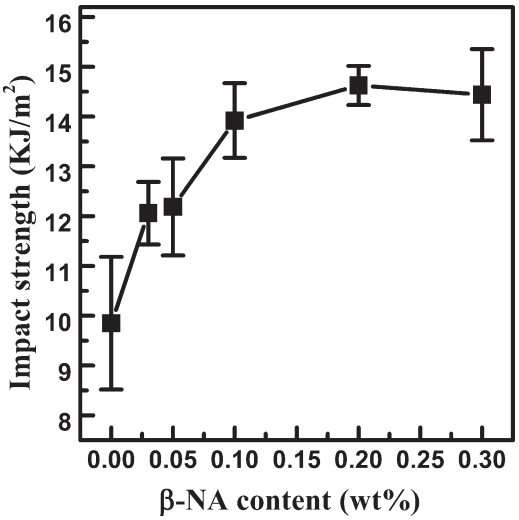

Figure 12. Charpy impact strengths of IPCs with various β-NA contents at 0°C.

Since IPCs usually have better impact property at low temperature than PP, the impact strengths of β-nucleated IPCs were measured at 0°C. It is observed that the impact strength increases greatly with the β-NA content when the β-NA content is in the range of 0–0.20 wt %. As compared with the IPC without β-NA, the impact strength of the IPC with 0.10 wt % β-NA is enhanced as much as 40%. When the β-NA content exceeds 0.20 wt %, the effect of β-NA on the impact strength is insignificant. Such a result agrees well with the tanδ peak intensity measured by DMA. This shows that β crystal indeed has better impact property over α crystal. It should be noted that, the relative fraction of the β-crystal is approximately 94% and the overall crystallinity varies slightly when the β-NA content ranges from 0.03 to 0.30 wt %, but the impact strength is increased continuously with increasing the β-NA content until 0.20 wt % of β-NA content. This is probably because the macroscopic crystalline morphology still changes with the β-NA content (Figure 9), though the relative fraction of the β-crystal and the overall crystallinity are nearly invariant at high β-NA content. As a result, different factors, including the crystal structure, the macroscopic morphology and more inclusion of the amorphous component into the inter-lamellae induced by β-NA, may be responsible for the improvement of the impact property. We can see from the DMA and impact strength that the suitable amount of β-NA is about 0.05–0.1 wt % for this IPC.

CONCLUSIONS

The above results show that calcium tetrahydrophthalate is a highly efficient β-NA for IPC. The relative fraction of β crystal can reach 93.5% upon addition of 0.03 wt % of β-NA. During non-isothermal crystallization process, the relative fraction of β-crystal strongly depends on the cooling rate. A faster cooling rate leads to a lower fraction of β-crystal. Isothermal crystallization kinetics show that β-NA can greatly enhance the number of crystal nuclei and the Avrami exponent, leading to a faster overall crystallization rate, as compared with the IPC without β-NA. More amorphous components are included into the inter-lamellae. DMA test reveals that the storage modulus at low temperature and the intensity of the tanδ peak from PP first increase with the β-NA content and reach a maximum at 0.05–0.10 wt % β-NA. When a small amount of β-NA is added, the impact strength of IPC at 0°C can be greatly improved.

ACKNOWLEDGMENTS

This work was supported by National Basic Research Program of China (2011CB606005) and National Natural Science Foundation of China (51073138). The authors also would like to thank the beamline BL16B1 at SSRF for providing the beam time.

REFERENCES

1. Galli, P.; Vecellio, G. *Prog. Polym. Sci.* **2001**, *26*, 1287.
2. Dong, Q.; Wang, X. F.; Fu, Z. S.; Xu, J. T.; Fan, Z. Q. *Polymer* **2007**, *48*, 5905.
3. Xu, J. T.; Feng, L. X. *Eur. Polym. J.* **2000**, *36*, 867.
4. Xu, J. T.; Fu, Z. S.; Fan, Z. Q.; Feng, L. X. *Eur. Polym. J.* **2002**, *38*, 1739.
5. Fu, Z. S.; Fan, Z. Q.; Zhang, Y. Z.; Xu, J. T. *Polym. Int.* **2004**, *53*, 1169.
6. Fu, Z. S.; Xu, J. T.; Zhang, Y. Z.; Fan, Z. Q. *J. Appl. Polym. Sci.* **2005**, *97*, 640.
7. Cheruthazhekatt, S.; Pijpers, T. F. J.; Harding, G. W.; Mathot, V. B. F.; Pasch, H. *Macromolecules* **2012**, *45*, 5866.
8. Cheruthazhekatt, S.; Pijpers, T. F. J.; Harding, G. W.; Mathot, V. B. F.; Pasch, H. *Macromolecules* **2012**, *45*, 2025.
9. Tian, Z.; Gu, X. P.; Wu, G. L.; Feng, L. F.; Fan, Z. Q.; Hu, G. H. *Ind. Eng. Chem. Res.* **2011**, *50*, 5992.
10. Tian, Z.; Gu, X. P.; Wu, G. L.; Feng, L. F.; Fan, Z. Q.; Hu, G. H. *Ind. Eng. Chem. Res.* **2012**, *51*, 2257.
11. Fu, Z. S.; Tu, S. T.; Fan, Z. Q. *Ind. Eng. Chem. Res.* **2013**, *52*, 5887.
12. Mehtarani, R.; Fu, Z. S.; Tu, S. T.; Fan, Z. Q.; Tian, Z.; Feng, L. F. *Ind. Eng. Chem. Res.* **2013**, *52*, 9775.
13. Mehtarani, R.; Fu, Z. S.; Fan, Z. Q.; Tu, S. T.; Feng, L. F. *Ind. Eng. Chem. Res.* **2013**, *52*, 13556.
14. Cheruthazhekatt, S.; Harding, G. W.; Pasch, H. *J. Chromatogr. A* **2013**, *1286*, 69.
15. Cheruthazhekatt, S.; Mayo, N.; Monrabal, B.; Pasch, H. *Macromol. Chem. Phys.* **2013**, *214*, 2165.
16. Cheruthazhekatt, S.; Pijpers, T. F. J.; Mathot, V. B. F.; Pasch, H. *Anal. Bioanal. Chem.* **2013**, *405*, 8995.
17. Zhu, H. J.; Monrabal, B.; Han, C. C.; Wang, D. J. *Macromolecules* **2008**, *41*, 826.
18. Chen, R. F.; Shangguan, Y. G.; Zhang, C. H.; Chen, F.; Harkin-Jones, E.; Zheng, Q. *Polymer* **2011**, *52*, 2956.
19. Li, Y.; Xu, J. T.; Dong, Q.; Fu, Z. S.; Fan, Z. Q. *Polymer* **2009**, *50*, 5134.
20. Liu, Y. M.; Li, Y.; Xu, J. T.; Fu, Z. S.; Fan, Z. Q. *J. Appl. Polym. Sci.* **2012**, *123*, 535.
21. Liu, Y. M.; Xu, J. T.; Fu, Z. S.; Fan, Z. Q. *J. Appl. Polym. Sci.* **2013**, *127*, 1346.

22. Liu, Y. M.; Tong, Z. Z.; Huang, J.; Zhou, B.; Xu, J. T.; Fu, Z. S.; Fan, Z. Q. *Ind. Eng. Chem. Res.* **2013**, *52*, 16239.
23. Doshev, P.; Lohse, G.; Henning, S.; Krumova, M.; Heuvelsland, A.; Michler, G.; Radusch, H. J. *J. Appl. Polym. Sci.* **2006**, *101*, 2825.
24. Song, S. J.; Feng, J. C.; Wu, P. Y.; Yang, Y. L. *Macromolecules* **2009**, *42*, 7067.
25. Song, S. J.; Wu, P. Y.; Feng, J. C.; Ye, M. X.; Yang, Y. L. *Polymer* **2009**, *50*, 286.
26. Tong, C. Y.; Lan, Y.; Chen, Y.; Yang, D. C.; Yang, X. N. *J. Appl. Polym. Sci.* **2012**, *123*, 1302.
27. Remerie, K.; Groenewold, J. *J. Appl. Polym. Sci.* **2012**, *125*, 212.
28. Kock, C.; Gahleitner, M.; Schausberger, A.; Ingolic, E. *J. Appl. Polym. Sci.* **2013**, *128*, 1484.
29. Tan, H. S.; Li, L.; Chen, Z. N.; Song, Y. H.; Zheng, Q. *Polymer* **2005**, *46*, 3522.
30. Rungswang, W.; Plailahan, K.; Saendee, P.; Rugmai, S.; Cheevasrirungruang, W. *Polymer* **2013**, *54*, 3699.
31. Rungswang, W.; Saendee, P.; Thitisuk, B.; Pathaweeisariyakul, T.; Cheevasrirungruang, W. *J. Appl. Polym. Sci.* **2013**, *128*, 3131.
32. Ruff, M.; Lang, R. W.; Paulik, C. *Macromol. React. Eng.* **2013**, *7*, 328.
33. Kock, C.; Aust, N.; Grein, C.; Gahleitner, M. *J. Appl. Polym. Sci.* **2013**, *130*, 287.
34. Varga, J. *J. Macromol. Sci.-Phys.* **2002**, *B41*, 1121.
35. Grein, C. *Adv. Polym. Sci.* **2005**, *188*, 43.
36. Luo, F.; Geng, C. Z.; Wang, K.; Deng, H.; Chen, F.; Fu, Q.; Na, B. *Macromolecules* **2009**, *42*, 9325.
37. Xiao, W. C.; Feng, J. C. *J. Appl. Polym. Sci.* **2010**, *117*, 3247.
38. Fan, J. S.; Feng, J. C. *Ind. Eng. Chem. Res.* **2013**, *52*, 761.
39. Luo, F.; Xu, C. L.; Wang, K.; Deng, H.; Chen, F.; Fu, Q. *Polymer* **2012**, *53*, 1783.
40. Li, X. X.; Wu, H. Y.; Chen, J. W.; Yang, J. H.; Huang, T.; Zhang, N.; Wang, Y. *J. Appl. Polym. Sci.* **2012**, *126*, 1031.
41. Luo, F.; Xu, C. L.; Ning, N. Y.; Wang, K.; Deng, H.; Chen, F.; Fu, Q. *Polym. Int.* **2013**, *62*, 172.
42. Cheng, D.; Feng, J. C.; Yi, J. J. *J. Appl. Polym. Sci.* **2012**, *123*, 1784.
43. Li, J. X.; Cheung, W. L.; Jia, D. M. *Polymer* **1999**, *40*, 1219.
44. Zhao, S. C.; Cai, Z.; Xin, Z. *Polymer* **2008**, *49*, 2745.
45. Su, Z. Q.; Dong, M.; Guo, Z. X.; Yu, J. *Macromolecules* **2007**, *40*, 4217.
46. Phillips, A.; Zhu, P. W.; Edward, G. *Polymer* **2010**, *51*, 1599.
47. Labour, T.; Vigier, G.; Seguela, R.; Gauthier, C.; Orange, G.; Bomal, Y. *J. Polym. Sci. Part B: Polym. Phys.* **2002**, *40*, 31.
48. Zhang, Z. S.; Wang, C. G.; Meng, Y. Z.; Mai, K. C. *Compos. A: Appl. Sci. Manuf.* **2012**, *43*, 189.
49. Ding, Q.; Zhang, Z. S.; Wang, C. G.; Jiang, J.; Li, G.; Mai, K. C. *Thermochim. Acta* **2012**, *536*, 47.
50. Guan, Z. X.; Lin, Z. D.; Mai, K. C. *Compos. Sci. Technol.* **2013**, *87*, 58.
51. Menyhard, A.; Varga, J.; Molnar, G. *J. Therm. Anal. Calorm.* **2006**, *83*, 625.
52. Varga, J.; Menyhard, A. *Macromolecules* **2007**, *40*, 2422.
53. Dong, M.; Gu, Z. X.; Yu, J.; Su, Z. Q. *J. Polym. Sci. Part B: Polym. Phys.* **2008**, *46*, 1725.
54. Dou, Q. *J. Appl. Polym. Sci.* **2009**, *111*, 1738.
55. Zhan, K. J.; Yang, W.; Yue, L.; Xie, B. H.; Yang, M. B. *J. Macromol. Sci. B Phys.* **2012**, *51*, 2412.
56. Feng, J. C.; Duan, Y.; Jiao, Y.; Zhang, X. J.; Chen, M. C. *Acta Phys. Chim. Sin.* **2005**, *21*, 1431.
57. Xiao, W. C.; Wu, P. Y.; Feng, J. C.; Yao, R. Y. *J. Appl. Polym. Sci.* **2009**, *111*, 1076.
58. Chinese Pat. CN 102181092A.
59. Shangguan, Y. G.; Song, Y. H.; Peng, M.; Li, B. P.; Zheng, Q. *Eur. Polym. J.* **2005**, *41*, 1766.
60. Turner-Jones, A.; Aizlewood, J. M.; Beckett, D. R. *Makromol. Chem.* **1964**, *75*, 134.
61. Lotz, B. *Polymer* **1998**, *39*, 4561.
62. Wang, C. G.; Zhang, Z. S.; Mai, K. C. *J. Therm. Anal. Calorim.* **2011**, *106*, 895.
63. Xu, X. R.; Xu, J. T.; Feng, L. X.; Chen, W. *J. Appl. Polym. Sci.* **2000**, *77*, 1709.
64. Tong, Z. Z.; Huang, J.; Zhou, B.; Xu, J. T.; Fan, Z. Q. *Macromol. Chem. Phys.* **2013**, *214*, 605.
65. Tong, Z. Z.; Xu, J. T.; Xia, S. J.; Fan, Z. Q. *Polym. Int.* **2013**, *62*, 228.
66. Tong, Z. Z.; Zhou, B.; Huang, J.; Xu, J. T.; Fan, Z. Q. *Macromolecules* **2014**, *47*, 333.